J. Fluid Mech. (2009), *vol.* 621, *pp.* 183–204.
doi:10.1017/S0022112008004771 Printed in the United Kingdom

A branched one-dimensional model of vessel networks

JOSE-MARIA FULLANA[1] AND STÉPHANE ZALESKI[2,3,†]

[1] Service de Biophysique, Laboratoires Innothera, F-94110 Arcueil, France

[2] UPMC Univ Paris 06, UMR 7190, Institut Jean Le Rond d'Alembert, F-75005 Paris, France

[3] CNRS, UMR 7190, Institut Jean Le Rond d'Alembert, F-75005 Paris, France

(Received 17 July 2006 and in revised form 16 October 2008)

We introduce a model representing the venous network of the leg. The network consists of a coupled system of elastic tubes. The flow through each elastic tube is assumed to be unsteady, incompressible and one-dimensional. The network topology, as well as the lengths and diameters of the tubes, is based on literature data. As in the human leg the network is composed of two sub-networks, deep and superficial, which are connected by transverse segments. We introduce a new model for confluences or branching points, as well as models of the valvular system and of the muscular activity. We perform a numerical study of the transmission and reflection of waves at a confluence. Our model valvular system imposes a privileged direction of the flow towards the heart. Muscular activity is modelled using a modification of the tube law of the vessel and through an inflow of blood when muscle contraction pushes blood from the microcirculation to the veins. The model is capable of simulating several motions such as walking, dorsal flexion and tiptoe. Numerical tests show the physical relevance of the model, and in particular demonstrate that when the system is excited at the foot level, a two-frequency response appears. These frequencies are closely related to the characteristic lengths of the typical segments of the deep and of the superficial networks. We find good qualitative agreement between experimental and numerical flow rates, using clinical data corresponding to a single 'tiptoe' motion. We make numerical predictions of the internal venous pressure at the foot level in a valvular-incontinent system which agree with clinical observations.

1. Introduction

In the human cardiovascular system, local flow features may have global effects on the circulatory flow. For example, flow modifications caused by atherosclerosis, stenosis or aneurysms cause modifications of the shear stress on the vessel walls which in turn produce changes in the mechanical characteristics of the vessels. This implies alterations in local vessel compliance, local flow resistance, wave transmission and consequently significant modifications of the macrocirculation (Falson *et al.* 1998).

Numerical simulations help to acquire knowledge about the local and global features of the circulatory network. In particular, numerical simulations provide a useful approach for understanding the human cardiovascular system. In the past, simple models for single vessels have been used to describe blood flow in arteries and veins. These models include (i) lumped models, i.e. the model is spatially homogeneous, Bertram

† Email address for correspondence: stephane.zaleski@upmc.fr

& Pedley (1982) is a good reference, or (ii) one-dimensional linear and nonlinear models based on partial differential equations (Cancelli & Pedley 1985; Matsuzaki & Matsumoto 1989; Kamm & Pedley 1989; Elad *et al.* 1991; Brook 1997). In all cases these models involve averaged quantities (area, velocity and pressure).

Another possibility is to perform a three-dimensional numerical analysis which would provide a very detailed view of local flow features such as flow recirculation, shear stress or tracer transport. However, extensive computational resources are necessary and a fully three-dimensional approach of a venous or arterial network would be prohibitively expensive on present-day computers, at least for the frequent and diverse simulations that a systematic study of the leg hemodynamics would require. The computational study of Stokes flow (Heil & Pedley 1996) or Navier–Stokes flow (Rosar & Peskin 2001; Marzo, Luo & Bertram 2005) through a collapsible tube is indeed a task of large magnitude. The three-dimensional approach remains nevertheless necessary to understand the real flow behaviour in vessels and could be coupled with zero and/or one-dimensional models (Formaggia *et al.* 1999, 2001; Fernandez, Milisic & Quarteroni 2005).

The elementary lumped models of circulatory networks considered in the literature are based on the electrical analog of the system (Westerhof *et al.* 1969; Avolio 1980). In this approach each vessel is modelled by a basic element composed of resistances, inductances and capacitances. Researchers were able to simulate the human macrocirculation by connecting in a network several of these elements. Although these networks can be complex, their numerical computation is fast and effective. The pitfall is that they are unable to take into account important features such as wave propagation along elongated vessels. Another important drawback is that it is often difficult to make a quantitative connection between measured mechanical properties (e.g. compliance) and model results. In spite of that, they are still used to prescribe boundary conditions and for multiscale modelling (Formaggia *et al.* 1999; Quarteroni & Formaggia 2003).

An alternative to the lumped model is a network of tubes or segments, each described by a spatially one-dimensional system of partial differential equations. The model we present in this paper is of this type. Most of such models are built using one-dimensional continuity and momentum equations (Stergiopulos, Young & Rogge 1992; Olufsen *et al.* 2000*a*; Ozawa *et al.* 2001). A more sophisticated alternative approach is to use the method of characteristics (Sherwin *et al.* 2003; Wang & Parker 2004) which can compute linear or nonlinear solutions for wave motion in arteries. We note that, in the arterial case, the problem of the direction of the characteristics in the hyperbolic formulation is simplified by the relative weakness of backflows, while in the venous case there may be in exceptional circumstances both backflows and large velocities that make the direction of characteristics uncertain.

Experimental observations of the venous network show differences with the arterial one: the veins are more compliant so the rigid or quasi-rigid hypothesis used in arterial research does not apply. Moreover, healthy veins of the leg have valves to keep the blood circulation oriented towards the heart, preventing backflows. Finally, the veins of the leg have a dynamic environment as a consequence of the contractions of the surrounding muscles.

Muscular contractions play an important role in venous return because they compress the deep veins of the calf. When this compression occurs the distal valve of the deep vein as well as the valves of the perforating veins closes. Blood is then ejected towards the heart. When the compression relaxes a reduction of pressure takes place in the deep veins and blood is aspirated into these veins through the perforating veins

located in the muscle compartments. The compression–relaxation mechanism reduces the intravenous pressure preventing the occurrence of high ambulatory pressures. In particular, this 'muscular pump' is responsible for the reduction of the ambulatory venous pressure (AVP). The AVP is defined as the minimal internal pressure at the distal marginal vein (MV), a superficial vein located at the upper surface of the foot, and it is an important marker of venous disease. When there is an abnormal muscular pump or valvular incontinence, the AVP rises and produces an ambulatory hyper-pressure.

In order to study these issues, we designed a numerical model of the venous network of the leg. The model is a system of coupled elastic tubes. Each elastic tube represents a venous vessel. Flow through the tubes is assumed to be unsteady, incompressible and one-dimensional. The fluid–structure interaction between the flow and the wall is modelled by a relation between tube area and the difference between internal and external pressures. This relation, called the tube law, can be given *a priori* in analytical form or fitted from experimental data. We assume that, provided with a correct tube law, the one-dimensional numerical system can represent flow dynamics in a vessel. There have been numerous studies of flow in elastic and collapsible tubes, with applications to flows through arteries, veins, bronchi or the urethra (Griffiths 1971; Young & Tsai 1975; McClurken *et al.* 1981; Jan, Kamm & Shapiro 1983; Elad, Kamm & Shapiro 1987; Kamm & Pedley 1989). These flexible-tube models have been successfully compared to controlled experiments (Kamm & Shapiro 1979; Jan *et al.* 1983; Fullana *et al.* 2003; Cros 2003) where experimental data on flow rate and pressure were compared to numerical solutions. On the lower leg in particular, numerical simulations of the external compression activity can be found in Kamm (1982) and Dai, Gertler & Kamm (1999).

Our numerical network also includes a model of muscular activity and a model of valve activation. Muscular activity and valves are specific and important features of the venous network, whereas they are not needed, for instance, in a model of the arterial network. We define a few 'compartments' or zones containing muscles with the same muscular activity. The choice of compartments attempts to match human physiology. Valves are necessary to keep the blood flow in the right direction. They are present in each segment of the leg: in vertical segments to let the blood flow from the foot to the heart and in horizontal segments to collect the superficial circulation into the deep network. We also define a new approach for branching points or confluences. In our formulation, they are modelled as a soft tank with n entries or branches each corresponding to a venous segment.

The paper is organized as follows: in § 2 we describe the mathematical models for a single vessel, a confluence, a valve and for muscular activity. We also describe the venous network and its boundary conditions. Numerical results are presented in § 3 where we study the confluence model, the wave reflection at the confluences and the exit condition of the network. Then we compute network solutions using an experimental venous law, and compare numerical results to experimental data for a tiptoe. We also describe numerical predictions for the internal pressure at the foot level in a valvular incontinent system.

2. Models

2.1. *Vessel model*

We assume an unsteady, incompressible one-dimensional flow through a collapsible tube. The length scale for the variation of the tube cross-section shape, velocity and pressure is large compared to the diameter of the tube. This assumption may fail in

some cases, for instance near the ends of the tubes where they attach to the confluences. However, these regions are limited in size and the simplification is so useful that it is very difficult to consider an alternative. Moreover, detailed comparisons between experiments and numerical simulations support this assumption (Fullana *et al.* 2003). This also means that transverse variations of pressure are neglected.

Therefore, we consider the flow as one-dimensional along the axis x: the pressure $p(x,t)$ and the velocity $U(x,t)$ are averaged values of the local variables over each cross-section. We note $A(x,t)$ the area of the cross-section at x and t. Longitudinal non-uniformities in the tube shape result in gradients of the area $A(x,t)$.

The governing equations for the fluid flow express conservation of mass (Shapiro 1977)

$$\frac{\partial A}{\partial t} + \frac{\partial}{\partial x}(AU) = q, \tag{2.1}$$

where $q = q(x,t)$ is the source term that corresponds to the microcirculatory flow. Conservation of momentum gives

$$\rho\frac{\partial U}{\partial t} + \alpha\rho U\frac{\partial U}{\partial x} = -\frac{\partial p}{\partial x} - \rho g\sin\theta - f_v, \tag{2.2}$$

where ρ is the density, g is gravity and θ stands for the angle between the tube axis and the horizontal. The coefficient α depends on the velocity profile in the tube. For a uniform velocity profile as expected at high Reynolds number with negligible boundary layers $\alpha = 1$, while for the axisymmetric Poiseuille flow expected at low Reynolds number $\alpha = 4/3$. However at small Reynolds number the nonlinear, inertial term is small compared to the viscous term. As a reasonable simplification we set $\alpha = 1$. A derivation of (2.2) is given by Anliker, Rockwell & Ogden (1971) or Quarteroni & Formaggia (2003).

The viscous effects are included in f_v, which may be obtained from solutions of the Navier–Stokes equations for parallel flow in tubes of given cross-section (Cancelli & Pedley 1985). For example, for laminar flow ($Re < 4000$) and $A > A_0$ the momentum loss is $f_v = 8\pi\mu A^{-1}U$. For the laminar flow and $A < A_0$, if the tube is assumed to have elliptic cross-section then $f_v = 8\pi\mu A_0 A^{-2}U$ where μ is the fluid viscosity (Wild, Pedley & Riley 1977). A remarkable, and probably unrealistic feature of this expression for f_v is that it diverges for $A \to 0$. Thus we use instead a semi-analytical expression given by Ribreau, Naili & Langlet (1994). It assumes cross-section shapes deduced from thin-shell theory. Ribreau's expression involves a simple polynomial function $\mathscr{F}$, which is chosen so that it yields a good fit to experimental data. In this model $f_v(A, U; \mu, A_0) = (8\pi\mu U/A)\mathscr{F}(A/A_0)$ where

$$\mathscr{F} = \begin{cases} a_c, & \text{if } A < A_l, \\ \sum_{n=0}^{3} a_n (A/A_0)^n, & \text{if } A_l < A < A_0, \\ 1, & \text{if } A > A_0, \end{cases} \tag{2.3}$$

where $a_c, a_0, \ldots, a_3$ are scalar coefficients, which are constrained so that $\mathscr{F}$ is continuous. For instance $\sum_{i=0}^{3} a_i = 1$ so that $\mathscr{F}$ is continuous at 1. The value A_l is computed from the osculatory pressure when contact occurs along a straight line between opposite parts of the vessel walls. The values of $(a_c, A_l/A_0, a_0, a_1, a_2, a_3)$ are given by Ribreau *et al.* (1994) for different values of the initial ellipticity, the ellipticity being the ratio between the minor and major axes. For our case, the value of initial ellipticity is 1, and $(a_c, A_l/A_0, a_0, a_1, a_2, a_3) = (31.92, 0.21, -0.91, 9.35, -12.99, 5.55)$.

(It should be noted that the region $A < A_0$ is seldom relevant: the veins of the leg are usually inflated because of hydrostatic pressure.)

To close the system of equations (2.1) and (2.2), we use the mechanical characteristics of the veins. In this paper, we work with two different approaches: an analytic relation for elastic tubes used for numerical tests and validations on the one hand and an experimental relation used for experimental comparisons on the other.

The analytic tube law is described by

$$p - p_e = K_p P(A), \tag{2.4}$$

where K_p is a constant proportional to the bending stiffness and p_e is the external pressure. Additional physical effects such as the inertia of the surrounding tissue, or their viscosity, may be modelled in the tube law, which then becomes a differential equation.

The function $P(A)$ represents the effect of transverse stresses. Usually we write

$$P(A) = \begin{cases} A/A_0 - 1, & \text{if } A/A_0 > 1, \\ \frac{2}{3}[1 - (A/A_0)^{-3/2}], & \text{if } A/A_0 < 1, \end{cases} \tag{2.5}$$

where A_0 is the cross-sectional area at $p - p_e = 0$. A closely related concept is the compliance $\mathscr{C} = \mathrm{d}A/\mathrm{d}P$. When dilated ($A > A_0$) the tube has circular cross-section and constant compliance. The tube starts to collapse at $A = A_0$. As A decreases the tube becomes increasingly elliptical and compliance steadily declines. As the collapse intensifies, opposite sides of the wall come into contact and two parallel conduits are formed. Compliance falls further and the cross-section is reduced in size but the pressure remains self-similar of the form $P(A) \simeq -(2/3)(A/A_0)^{-3/2}$ (Fung 1996). The tube law determines the speed $c = \sqrt{A(K_p/\rho)\mathrm{d}P/\mathrm{d}A}$ of small perturbations (see the Appendix).

For the experimental tube law, a clinical procedure was developed to determine the relationship $P(A)$ for each vein type in the deep and superficial bed (Bassez, Chauveau & Flaud 2001). A transverse echographic scanner was used to measure the cross-section area A for different external pressures p_e. The measurement data allow to build a tube law for each vein. We expect the use of the experimentally determined tube law to considerably improve the realism of our model, and to be critical in the ability to obtain satisfactory comparisons between clinical studies and model predictions.

2.2. *Confluence model*

A confluence model is a manner to couple the fluid-dynamical equations (2.1–2.2) describing the segments connected through the confluence. Since the fluid-dynamical equations are hyperbolic and of second order, the solution of the equations in the segments requires one boundary condition for each characteristic line entering the segment. In the subcritical regime, this means one boundary condition on each side of the segment. Thus, at a confluence with n branches, one must determine n quantities, one for each segment. The simplest way is to use one condition for the conservation of mass and $n - 1$ for the conservation of energy. For example, for a three-branch bifurcation we have from conservation of mass

$$q_1 + q_2 + q_3 = 0, \tag{2.6}$$

where $q_i = A_i U_i$ at the bifurcation, and the Bernoulli-type conditions

$$p_1 + \rho U_1^2/2 = p_2 + \rho U_2^2/2, \tag{2.7}$$

$$p_1 + \rho U_1^2/2 = p_3 + \rho U_3^2/2, \tag{2.8}$$

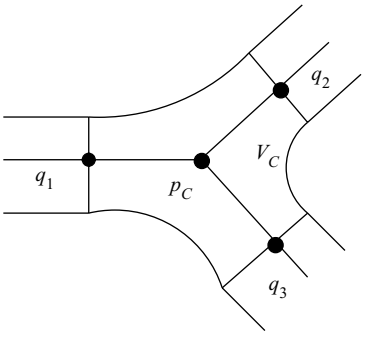

FIGURE 1. Model of confluence with three branches. Each flow rate q_i is computed from the difference between pressure at the confluence centre and pressure in neighbouring vessels. Mass conservation yields the confluence volume V_C. The confluence pressure p_C is determined from V_C assuming a compliant wall.

which state that the three stagnation pressures are equal. In this 'energy-conserving' approach head losses are neglected, and many authors have discussed the need to add a model for these losses.

There is a large literature on confluences, some of which is motived by research on arterial flow: Stettler, Niederer & Anliker (1981); Stergiopulos *et al.* (1992); Olufsen (1999, 2000); Olufsen *et al.* (2000*b*); Wan *et al.* (2002); Sherwin *et al.* (2003); Bernhard *et al.* (2005). These papers provide numerous examples of the behaviour of the dynamical variables (area, velocity and pressure) across the confluence.

To estimate the singular head losses, we can refer to the work of Cros (2003). He has done numerical simulations of confluences of rigid pipes for different angles and diameter ratios and the conclusion was that in the leg's venous network the singular pressure head loss can be neglected (angles in the leg run between 10° and 45°, except for the perforating veins which have an angle of 90° but a very small velocity, and the diameter ratios are on average close to 1). This conclusion agrees with Olufsen *et al.* (2000*b*) where a non-zero loss coefficient was used only in the bifurcation from the ascending aorta in the aortic arc.

Our formulation differs from the previous ones in the literature, as in our case the confluence is an elastic tank of small size. This tank has n entries or arms each corresponding to a segment of the network. A confluence is characterized by a volume V_C, a pressure p_C and its entry flow rates $q_1, \ldots, q_n$ (figure 1). This description needs to be connected to the discretization of each neighbouring segment, which we will describe below together with the numerical method. This new approach to the modelling of confluences could be applied to any network of elastic tubes, including arterial networks.

2.3. *Valve model*

In the general circulation the vein valves are necessary to keep blood flowing towards the heart and against the force of gravity. Mathematically, valves are singular points in the circuit, allowing a pressure jump across that point. Figure 2 shows a simple sketch of valve behaviour. In case (*a*) the local pressure gradient is favourable; therefore the flow goes naturally towards the heart. In case (*b*) the flow is stopped, and $U = 0$ at this point. Numerically, if one suddenly imposes the singular condition $U = 0$ numerical instabilities may be produced. Moreover, echo-Doppler investigations show that real valves allow a small reflux or backflow. We modify the equations to include a very

FIGURE 2. Sketch of valve behaviour. (*a*) $p_+ > p_-$; (*b*) $p_+ < p_-$.

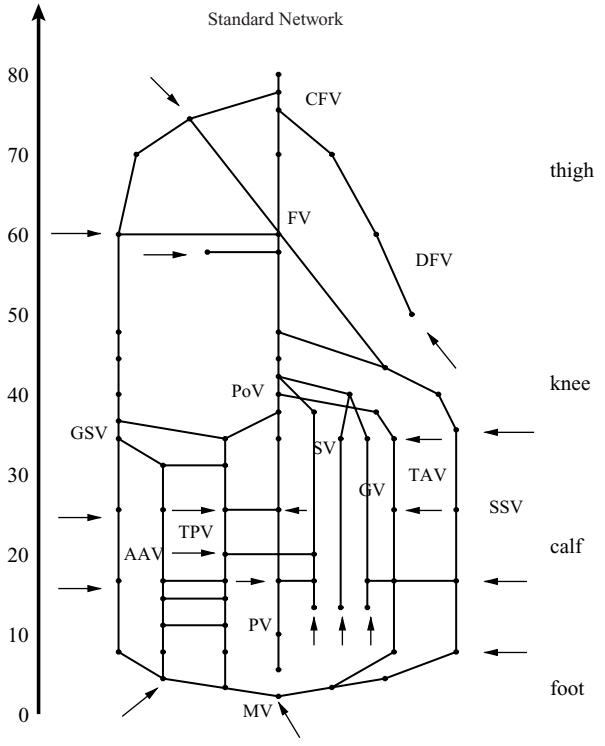

FIGURE 3. Two-dimensional diagram of the network of the lower limb. GSV, great saphenous vein; SSV, small saphenous vein; PV, peroneal vein; FV, femoral vein; CFV, common femoral vein and DFV, deep femoral vein. Arrows represent the location of the microcirculatory contribution, the two main contributions are those coming from the foot (zero altitude) and the thigh (DFV).

large, but not infinite, resistance to backflow through the valve. It will be convenient to use the indices + and − to denote values at points above and below the valve. Then

$$p_+ - p_- = -\rho K_{valve} U, \tag{2.9}$$

where U is the local velocity at the valve point, and K_{valve} is a very large coefficient representing the resistance when flow is forced in the 'forbidden' direction. This model yields a small residual reflux.

2.4. *Topography of the network model*

To obtain a model reflecting accurately the real venous topography, a vein is sometimes composed of several model venous segments. Each segment links a pair of nodes. The model topology as well as the length and diameter of each vein was based on literature data (Avolio 1980). The network is depicted in figure 3 where the altitude in cm and the corresponding zones in the leg: foot, calf, knee and thigh are shown on the left and the right, respectively.

Veins	Distal (cm)	Proximal (cm)
Great saphenous vein (GSV)	0.30	0.55
Peroneal vein (PV)	0.20	0.80
Small saphenous vein (SSV)	0.20	0.30
Common femoral vein (CFV)	0.85	1.00
Femoral vein (FV)	0.80	0.85
Deep femoral vein (DFV)	0.50	0.80

TABLE 1. Distal and proximal diameters of principal veins at zero transmural pressure.

From the plantar veins (marginal veins, MV), two superficial beds were defined as the great saphenous vein (GSV) and the small saphenous vein (SSV) on the left and the right of figure 3. The GSV was duplicated at the calf level giving the anterior accessory vein (AAV). The two superficial beds were connected to the deep network by the perforating veins (the horizontal segments). From left to right in the calf region, the full list is: GSV and AAV, tibial posterior vein (TPV), peroneal vein (PV), soleus vein (SV), two gastrocnemius veins (GV), tibial anterior vein (TAV), and finally the SSV. For the perforating veins, we have taken into account only the valvulated direct perforating veins of the largest diameter. The upper part of the network (the thigh model) was represented by the femoral branches: the femoral vein (FV), and common femoral vein (CFV), and by the deep femoral vein (DFV). The vein diameters of our standard network are given in table 1.

2.5. *Muscular pump and pulsating influx to the model*

Muscular contractions have two main effects. These contractions modify the stresses on the outer surface of the vessels. In some cases the effect is to modify the cross-sectional area of the vessels. This effect can be modelled by an increase in the external pressure of the tube law. The contractions also cause a fluid-mass influx coming from the blood pool of the muscular compartments. It is modelled by an increase in the source term $q(x,t)$ in the mass equation (2.1). We describe these two effects in turn.

The effect of the muscular contractions on the tube law can be modelled by a function $P_M(x,t)$ added to the external pressure p_e in (2.4),

$$p - p_e = P(A) + P_M(x,t). \tag{2.10}$$

From surface electromyography (EMG) measurements, we can approximate the shape of the function $P_M(x,t)$ (Alimi, Barthelemy & Juhan 1994). For numerical computations, we use two kinds of functions $P_M(x,t)$ (*a*) an impulse function to analyze the mechanical response of the network, and (*b*) an experimental function $P_M(x,t)$ coming from invasive pressure measurements of various muscular compartments (Maton *et al.* 2006*a*). We define three such compartments in the calf region (see figure 3):

(*a*) the tibial posterior compartment LPP (segments TPV and PV between the foot and the knee till the poplitean vein (PoV) including the corresponding perforating veins),

(*b*) the compartment including the muscle soleous and gastrocnemius, LPS (segments GV and SV between the foot and the knee till the PoV including the corresponding perforating veins),

(*c*) the tibial anterior compartment, LAE (the TAV segment between the foot and the knee till the PoV).

Modelling the increase in the source term $q(x,t)$ is performed by making it proportional to the function $P_M(x,t)$ described above.

2.6. *Boundary conditions*

The network has one influx condition and one exit boundary condition:

(*a*) for the venous flow coming from the microcirculation, from the muscular veins and the foot veins we suppose an inflow distribution along the network (at the foot, ankle and thigh level as shown by the arrows in figure 3), and we use the flow-rate values from the literature. In the simulations the total flow rate is set to 220 ml m^{-1}.

(*b*) the exit condition (at the CFV, the segment CFV in figure 3) is modelled by a virtual cava vein (not shown in figure 3) extending from the last node of the network to the heart. The heart pressure is maintained constant at 5 mmHg and the venous law (2.4) is modelled by a progressive neutral area A_0 growing from the distal to the proximal site. This approach avoids the wave reflections which would occur if we imposed a constant exit pressure. The imposed heart pressure attempts to model the actual right atrium pressure at the 'hydrostatic indifferent point'. At this point the pressure is not altered by postural changes and has small temporal variations (Guyton & Jones 1973). Considering no pressure variations in the vena cava and heart is nevertheless an approximation that we make. Adding some variations from breathing for instance could help explain some of the pulsatile character of the pressure measurements. However, in our approach, the pulsatile character of the model is ensured only by the muscular contraction model. In other words there is no pulsatile 'pulling' on the system, only pushing and squeezing.

3. Numerical results

3.1. *Numerical method*

The mathematical similarity with gasdynamics allows to reuse standard numerical methods. The classical MacCormack method (MacCormack 1969) has been developed for systems of conservation laws. It is a two-step predictor–corrector technique, with the following characteristics: it has an explicitly conservative form, and it uses a three-point spatial stencil and two time levels. It is second-order accurate in time and space. An approximate solution is obtained in the first step and then corrected in the second. This method of integration for hyperbolic equations was compared with others in Kimmel, Kamm & Shapiro (1988) and Elad *et al.* (1991). Though the choice of the difference approximation is not unique, in Peyret & Taylor (1983) a general formulation mixing forward and backward differences is used.

3.1.1. *MacCormack scheme*

We recall the MacCormack scheme. Equations (2.1–2.2) can be rewritten as

$$\partial_t Q = F(Q), \tag{3.1}$$

where the vector of unknowns is $Q = (A, U)$ and the term on the right-hand side contains derivatives with respect to x. The segments are discretized so that $Q_i(t) = Q(i\Delta x, t)$, where Δx is the mesh size. In this subsection, the indices i are increasing towards the heart. Derivatives inside F are discretized using biased finite

differences so that a backward-biased discrete approximation to F at point $x_i = i\Delta x$ is

$$F_i^- = \begin{pmatrix} -(A_i U_i - A_{i-1}U_{i-1})/\Delta x \\ -(U_i^2 - U_{i-1}^2)/(2\Delta x) - (p_i - p_{i-1})/(\rho\Delta x) - g\sin\theta_i - f_v(A_i, U_i)/\rho \end{pmatrix}, \quad (3.2)$$

where the p_i values are computed from the A_i using the tube law. The corresponding forward-biased derivative is noted F_i^+. Discretization in time is achieved by letting $Q_i^m = Q_i(m\Delta t)$ and

$$Q_i^* = Q_i^m + \Delta t F_i^+(Q^m), \quad (3.3)$$

$$Q_i^{m+1} = (Q^m + Q^*)/2 + (\Delta t/2)F_i^-(Q^*). \quad (3.4)$$

3.1.2. *Confluence scheme*

Near the confluence, we note the values such as $U_{0,k}$, $A_{0,k}$ at the nearest node from the confluence in branch k. In this subsection, we use spatial indices i increasing away from the confluence, so that velocity is counted positively when leaving the confluence. A problem arises when applying the MacCormack scheme at the $(0, k)$ nodes because $A_{-1,k}$, $U_{-1,k}$ are not defined. However, for all branches k we will take $p_{-1,k}$ to be the confluence pressure p_C, and $U_{-1,k}$ to be zero in the momentum equation. In the mass equation (that yields the derivative $\partial_t A_{0,k}$), the procedure is different and is explained below. First, we determine p_C as follows. The confluence volume is determined by mass conservation

$$\partial_t V_C = \sum_{k=1}^{n} - U_{0,k}A_{0,k} + q_{micro} \quad (3.5)$$

where q_{micro} stands for the microcirculatory contribution represented by arrows in figure 3. Second, the confluence pressure p_C is given by a volume law analogous to the vessel tube law

$$p_C = p_e + K_C P_C(V_C/V_0), \quad (3.6)$$

where P_C is a function that describes the compliance of the confluence. It is obtained by averaging the tube laws (2.4) of the neighbours. Moreover, V_0 is the reference volume for a given confluence. Finally, the constant K_C allows to adjust the confluence compliance, it is in general set to one, but it could be changed for instance to study a soft confluence coupling rigid veins. Below we will demonstrate by numerical simulations that the local dynamics is very sensitive to the reference volume V_0.

The mass equation cannot be solved with the backward-biased scheme because $U_{-1,k}$ is not defined. We thus determine $A_{0,k}$ by interpolation. A first method is to interpolate between the sections

$$A_{0,k} = \frac{1}{2}\left(A_{1,k} + A_0\frac{V_C}{V_0}\right). \quad (3.7)$$

A second method is to interpolate linearly the pressures, then to invert the tube law to find the section

$$A_{0,k} = P^{-1}\left\{\frac{1}{2}\left[P(A_{1,k}) + P_C\left(\frac{V_C}{V_0}\right)\right]\right\}, \quad (3.8)$$

where P and P^{-1} are the tube law and its inverse, and $P_C()$ is the function defined above. Numerical experiments show that the interpolation (3.8) is preferable to the interpolation (3.7) as it avoids pressure jumps.

As it stands, this scheme is consistent with an energy-conserving formulation as we now show. The above scheme yields in steady state $F^{-}_{0,k} = 0$, which implies

$$\frac{\rho U^2_{0,k}}{2} + p_k + (g \sin\theta_k - f_v/\rho)\Delta x = p_C. \tag{3.9}$$

Thus, p_C appears to be the stagnation point pressure. In the limit of small Δx

$$\frac{\rho U^2_{0,k}}{2} + p_k = p_C. \tag{3.10}$$

Thus, in steady state and with negligible head losses our formulation is equivalent to the energy-conserving approach (2.7). In unsteady situations, it may however be markedly different because the time derivatives will influence the confluence pressure and the mass conservation. Moreover, our formulation is not limited to the subcritical case where only n boundary conditions are needed for n branches, but would be equally applicable in the supercritical case.

3.2. *Results with an analytic tube law*

We present some numerical results: first we test the network elements (confluence volume, wave reflection and exit condition) using an analytic tube law and second we simulate venous network behaviour using an experimental venous law.

3.2.1. *Confluence volume*

We now discuss the important point of the confluence volume V_0 at zero transmural pressure. A reference value V_{0r} for the confluence volume is

$$V_{0r} = \sum_{k=1}^{n} A_{0,k}\Delta x, \tag{3.11}$$

where n is the number of vessels converging into a confluence and Δx is the same grid size used everywhere in the model. We show below the confluence dynamics for $n = 2$ and for departures from the reference value, everything being otherwise equal. The flow is going from left to right and has the form of a simple wave, which in the linearized approximation is $u(x, t) = t - x/c$ for $x < ct$ and $u = 0$ for $x > ct$. This wave is created imposing a velocity $u(0, t) = t$ on the leftmost node. We use the following analogy to explain the results: the wave represents a continuous train of pressure pulses representing each a volume differential δq; at the singular point (the confluence node) two extreme cases can appear:

(a) the volume V_0 is much smaller than the reference volume V_{0r} in (3.11); hence the volume differential δq carried by the wave creates a variation of the confluence volume V_C which is large compared to V_0. The confluence responds with a large pressure which perturbs the flow. This large pressure creates a source of flow at the confluence that appears as a perturbation of the wave patterns in figure 4(a);

(b) at the opposite, in the second case $V_0 \gg V_{0r}$, so the additional volume δq has a relatively small effect on the total volume V_0. The wave is delayed at the confluence as it takes time to fill the confluence, and a mild reflection of the incoming wave is seen propagating backwards. Figure 4(b) shows the response of the flow-rate profile for different times.

When we use $V_0 = V_{0r}$ for the confluence volume, the wave passes across without deformation as shown in figure 5(a). The conclusion is that V_0 should be adjusted depending on the nature of the reflections expected at confluences.

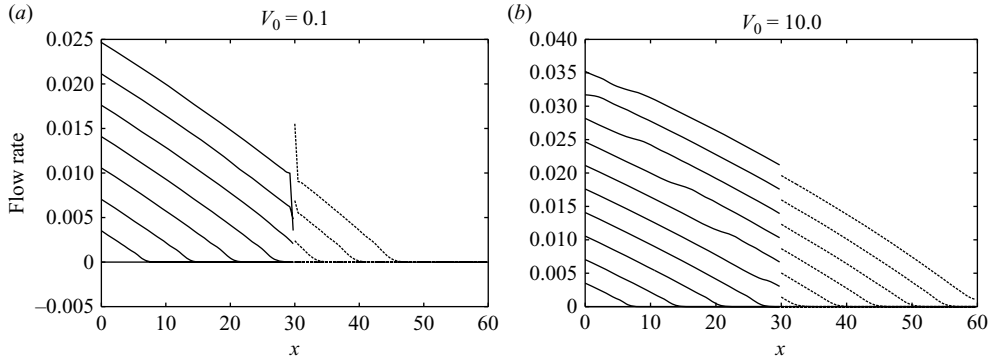

FIGURE 4. Flow rate profile for two values of the confluence volume V_0. The confluence is located at $x = 30$. The volume is smaller than (a), bigger than V_{0r} (b).

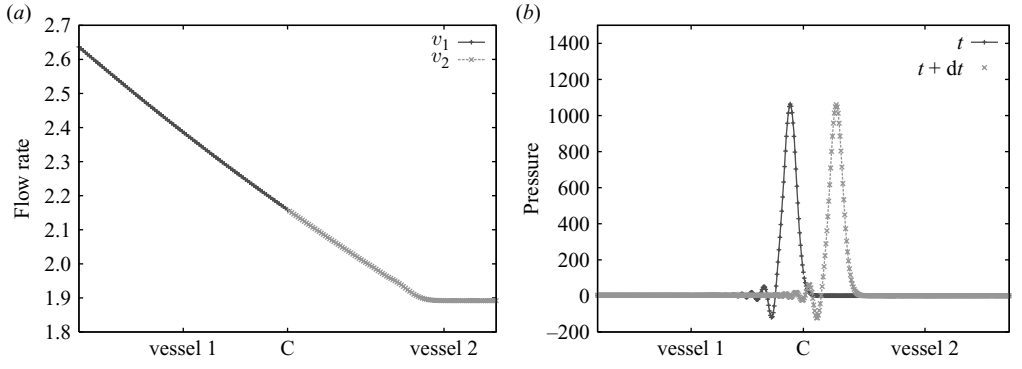

FIGURE 5. Two segments with a single confluence in between. (a) Flow rate AU as a function of position for two vessels connected by a confluence. (b) Pressure profile for two different times: before and after the confluence crossing. In both cases no wave reflection is seen.

Another point of view on our confluence model is that it is a numerical relaxation method with a characteristic time τ, which in steady outer conditions will converge to the classical equations (2.6–2.7). The volume V_0 controls the relaxation time τ. When the period or characteristic time of the wave is much larger than τ, the wave only 'sees' the steady state conditions (2.6–2.7). Large characteristic times τ may give different results, and correspond to large volumes V_0.

3.2.2. *Wave reflection*

In the Appendix we present a simple linear theory of wave reflection in confluences. In this section, we present some numerical results on a simple confluence composed of three segments. We use the analytic tube law (2.5) in the positive transmural pressure zone in two cases, a rigid compliance and a soft one. The two cases are $K_p = 30$ kPa and $K_p = 3$ kPa. We choose these values from experimental data which result in estimated values of K_p running between 50 kPa and 3 kPa (Bassez *et al.* 2001).

We present results for three cases.

(a) Case A: three segments with the same $K_p = 30$ kPa and the same neutral area $A_0 = 1\,\mathrm{cm}^2$;

(b) Case B: three segments with the same neutral area $A_0 = 1$ cm^2. One of the daughter segments has $K_p = 3$ kPa, and the two others have $K_p = 30$ kPa; and

	Case A		Case B		Case C	
	Theory	Numerical	Theory	Numerical	Theory	Numerical
R	−0.333	−0.333	−0.617	−0.617	−0.043	−0.042
T	0.666	0.666	0.382	0.382	0.957	0.958

TABLE 2. Theoretical and numerical values of the coefficients of wave reflection R and transmission T ratio in the three cases defined in the text.

(c) Case C: three segments with the same $K_p = 30$ kPa. One of the daughter segments has a neutral area $A_0 = 0.3$ cm^2 and the two others have neutral area $A_0 = 1$ cm^2.

Using these values of K_p and A_0 we computed the iterative admittance β for each segment from equation (A 6), which in turn allows to compute the ratio T between the amplitudes of transmitted and incoming waves (A 3) and the ratio R between the amplitudes of reflected and incoming waves (A 2). Both theoretical and numerical values of T and R are shown in table 2.

3.2.3. *Exit condition*

We study wave reflection near the exit point using a simple arrangement of two segments with one confluence between them. This represents the exit condition, the top segment representing the CFV placed at the top of figure 3.

The two vessels, vessel 1 and vessel 2, are connected by a confluence. Both vessels have the same tube law with $K_p = 30$ kPa and the neutral area $A_0 = 1$, but different lengths of 40 cm and 30 cm. The initial conditions are $u(x, t = 0) = C$ for all x where C is some constant.

For the first computation, the boundary conditions are: imposed velocity $u(0, t) = t + C$ on the input node of vessel 1 and fixed pressure at the exit of vessel 2 creating a wave as discussed above. Figure 5(a) shows the flow rate in both segments. The flow-rate wave passes through the confluence without changes. The zone with constant flow rate on the right of figure 5(a) has not yet been reached by the wave. We have also tested velocities larger than the physiological ones, and numerical results confirm that the numerical scheme is stable and suitable for the proposed model.

In a second computation, we impose a pressure pulse at the input node of vessel 1. Figure 5(b) shows the pressure profile at two different times: before and after the confluence crossing. The pressure pulse is not reflected at the confluence. We compute the reflection coefficient R and transmission coefficient T from (A 2) and (A 3) with two segments (therefore $\beta_3 = 0$) with $\beta_1 = \beta_2$, and we have $T = 1$ and $R = 0$. These values of T and R are consistent with the numerical solutions. Moreover, T and R were recomputed using the theory in (A 2) and (A 3), and using values of $A_{0,k}$ and $c_{0,k}$ computed at the confluence from the simulations. The result again agrees with the simulations.

3.3. *Results using experimentally measured tube laws*

In this section we use the full network and venous-tube laws obtained from the *in vivo* measurements of Bassez *et al.* (2001).

3.3.1. *Network response*

We simulate the action of the local foot pump by imposing a transient mass influx

$$q(t) = C[1 - \cos(\pi t/T)] \tag{3.12}$$

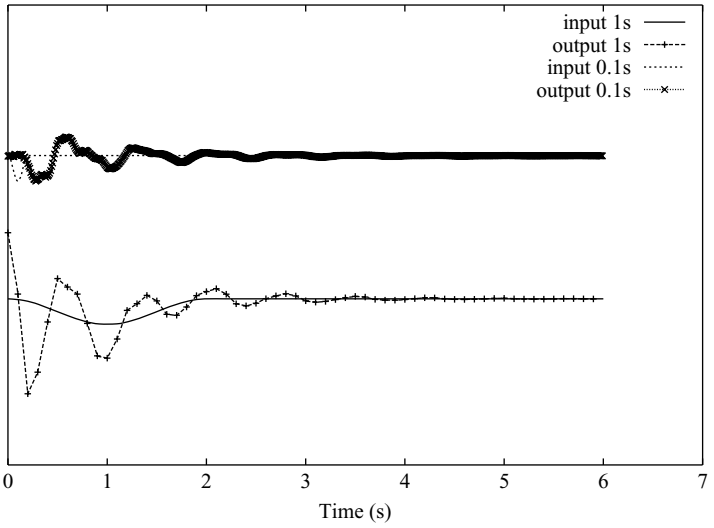

FIGURE 6. Comparison between two different imposed transient flow rates at entry. A transient flow rate of duration $T = 0.1$ s (upper) and $T = 1$ s (lower) (see text) is imposed at the foot level and shown in the figure. The corresponding responses (flow rates at the exit) are also shown. Vertical scale in arbitrary units.

for $0 < t < 2T$ and $q = 0$ otherwise, with C an arbitrary constant. Two cases are shown, one with $T = 0.1$ s and the other with $T = 1$ s. The influx is located at the foot level, specifically at the MV (see figure 3). Figure 6 shows the imposed mass flux rate $q(t)$ and the flow rate at the exit of the network for the two cases. Figure 6 shows that in the $T = 0.1$ case the deep veins are also excited and produce a second frequency in the response signal. This two-frequency response corresponds to a double-oscillatory system composed by the lower and upper limbs. The characteristic frequencies are closely related to their characteristic lengths. The numerical solution shows how the foot pump could play the role of an assistance system for the main heart pump by exciting the oscillatory system at the right frequency. Indeed, the networks of the upper and lower limbs can be considered as two weakly coupled systems. This prediction of a second frequency agrees with observations of physiology. Experimental data for dorsal flexion for a supine man from the clinical study of Maton *et al.* (2006*b*) show a second frequency that is not present in the muscular activity (figure 7). However, the manner in which the system is excited differs in the study of Maton *et al.* (2006*b*).

3.3.2. *Experimental comparison*

We now show the numerical predictions of our model for a tiptoe movement (straining upward on the tips of the toes). In a tiptoe movement many compartments are activated. We have experimental data on three different compartments: the tibial posterior compartment (LPP), the compartment including the muscle soleous and gastrocnemius (LPS), and the tibial anterior compartment (LAE). Figure 8 presents the temporal evolution of the intramuscular pressures (in mmHg) for the compartments. The muscular activity was measured by an invasive technique with a protocol approved by the Ethical Committee (CCPPRB Marseille I-No 02/19), a description of the protocol is given by Maton *et al.* (2006*a*).

The three pressure signals P_M are imposed in the corresponding compartments via (2.10). Figure 9 shows the flow rate at the exit at the Common Femoral Vein (CFV in figure 3) for the experimental data and its numerical prediction.

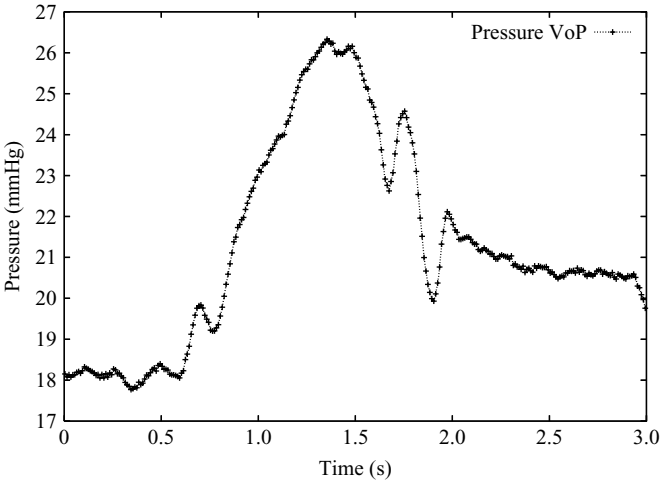

FIGURE 7. Experimental data for dorsal flexion. Pressure signal at the popliteal level.

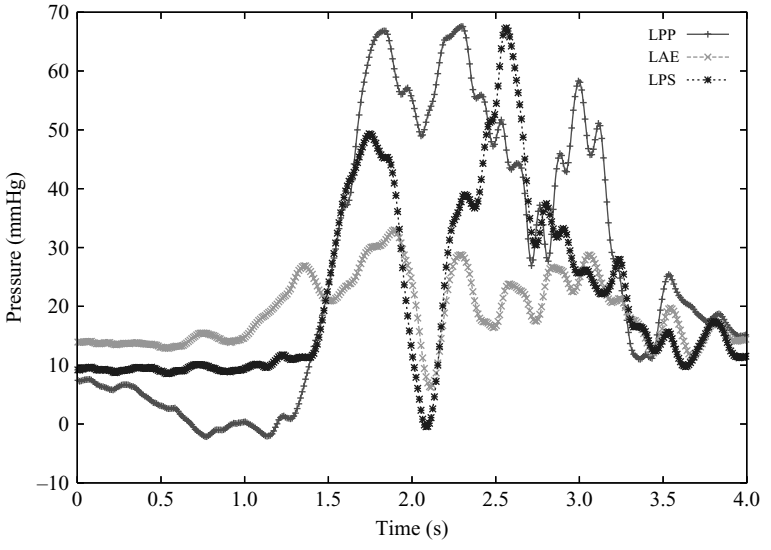

FIGURE 8. Muscular activation for the three compartments: the tibial posterior compartment (LPP), the compartment including the muscle soleous and gastrocnemius (LPS), and the tibial anterior compartment (LAE). Pressures are in mmHg.

For 2 s the two principal compartments LAE and the LPS dominate the dynamics. Even if LPS has greater values of pressure (maximum about 70 mmHg), the total volume of the LAE compartment is greater which makes LAE dominant in the dynamics. The sharp rise in flow rate at time 1.5 s is well modelled, but at later times the numerical results are less predictive.

At least two explanations may be advanced for the poor predictions: (i) the measurement point (CFV in figure 3) is far from the activated muscles and the experimental flow rate may be polluted by (*a*) wave reflections occurring at heterogeneities or confluences that are not modelled, and (*b*) spontaneous muscular activity, i.e. breathing, and (ii) the muscular activity of the thigh is not modelled in our approach. It may however be important due to its vicinity to the measurement point.

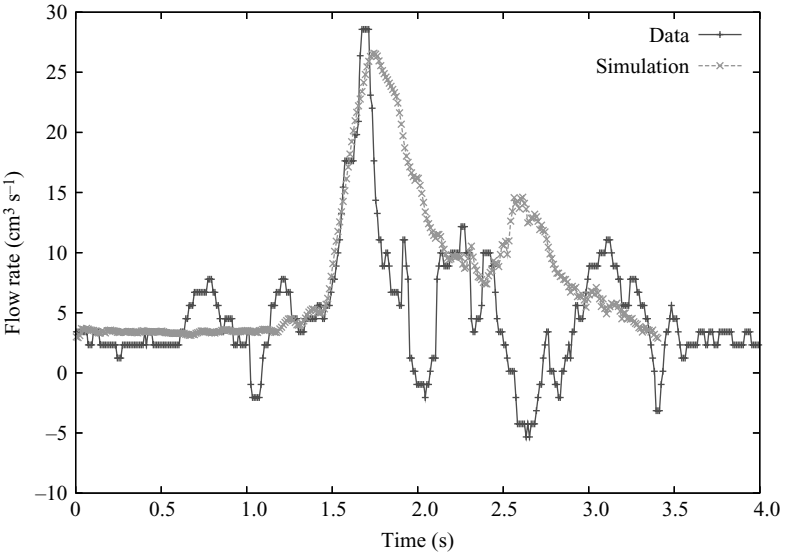

FIGURE 9. Flow rate at the exit of the network. Experimental data (crosses) and numerical results (solid line).

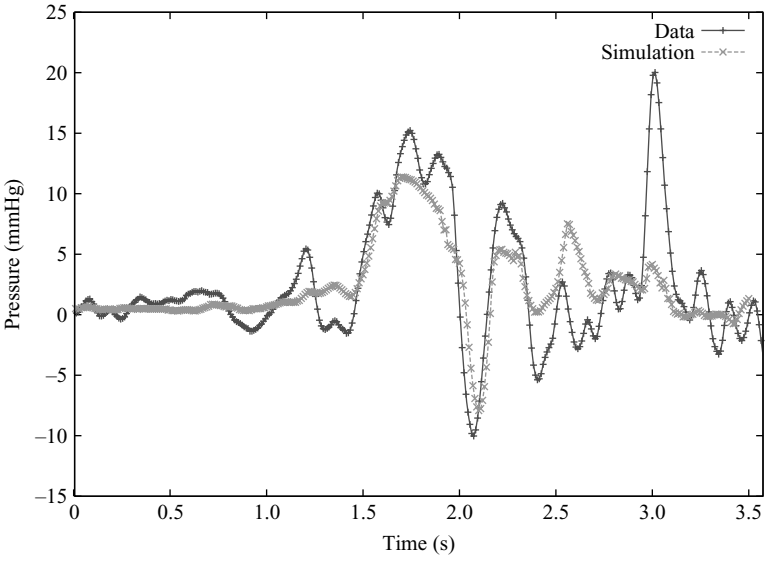

FIGURE 10. Temporal variation of the pressure at Popliteal level with respect to the pressure baseline. Experimental data (crosses+line) and numerical results (pluses+line).

Figure 10 shows the temporal variation of the pressure at the Popliteal level with respect to the pressure baseline (the hydrostatic pressure) for the experimental data and the numerical predictions. In this case the measurement point is located near the muscular activity (PoV at the knee level in figure 3) and the numerical predictions of the model are clearly improved.

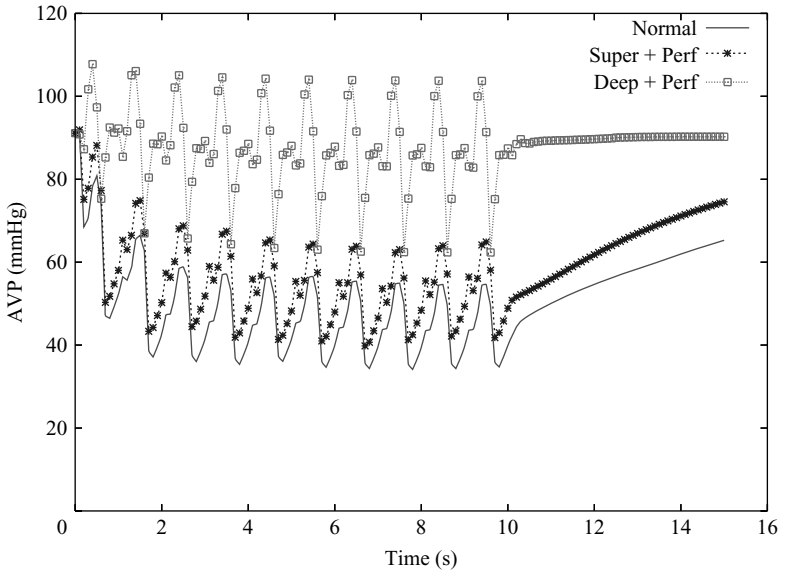

FIGURE 11. Time evolution of the ambulatory venous pressure (AVP): normal, superficial axis without valves and deep axis without valves. Pressure is in mm Hg; time is in seconds. The speed at which the pressure increases at the end of the walking sequence is an important marker of venous disease.

3.3.3. *Predictions on incontinent networks*

Finally, we present results on ambulatory venous pressure (AVP) in a protocol of 10 tiptoes. The AVP is defined as the minimal internal pressure at the distal Marginal Vein. It has higher values when the muscular pump is not functioning properly, for instance in case of valvular incontinence.

Figure 11 shows three cases: normal, with the superficial axis incontinent and with the deep axis incontinent. In a standing subject the AVP baseline is around 90 mmHg depending on the subject's height. During muscular activity it should fall to around 30–40 mmHg. In a protocol of 10 tiptoes, the largest pressure decrease is done for the 2–3 first movements, and the pressure becomes stable to give the AVP. Another important observable is the refilling time, the required time after muscular activity stops to reach the AVP baseline. Patients with muscular impairment or valve incontinence are hardly able to reduce the AVP and have a short refilling time. In a schematic manner, severe illness is correlated with a high AVP, a short refilling time and large pressure oscillations.

The numerical results agree with clinical data which show a rise in the AVP with the degree of incontinence (Nicolaides & Zukowski 1986). These results are used to design optimal compression profiles that reduce the ambulatory hyper-pressure by two mechanisms (i) increase of the viscous resistance, and (ii) restoration of valve functionality by the compression. This is one of the main applications of the present theoretical and numerical model.

4. Conclusion

We have described a theoretical and numerical model for simulating a circulatory network. The simulated network is a relatively detailed representation of the principal

veins of the leg. The topology of the network, the length and the diameter of the veins were based on literature data.

The model is based on a classical elastic tube approach, and the implementation of numerical confluences, valvules, and muscular activity. The flow through each elastic tube is assumed to be unsteady, incompressible, and one-dimensional. The resulting system of nonlinear equations is written in conservative form and solved using a MacCormack scheme.

We have presented a study of wave transmission and reflection in some simple configurations. Numerical results on reflection and transmission coefficients for two-way and three-way confluences are in agreement with theoretical results.

We investigate the system response to a transient entry flow rate modelling the foot pump. The system output shows two frequencies which are related to the lengths of the typical veins. We compare numerical results with experimental data for a single tiptoe movement. We report numerical predictions for the internal pressure at the foot level in a valvular incontinent system which agrees with clinical observations.

Improvements to the approach would involve a better modelling of singular head losses at confluences, a deeper study of wave reflection at confluences with comparisons to physiology and taking into account non-Newtonian characteristics of the blood. Indeed the one-dimensional approach ignores three-dimensional effects such as recirculation and secondary flows. This implies that the energy losses are not taken into account by the one-dimensional equations. However, empirical singular-head-loss coefficients could be used to avoid this pitfall. The non-Newtonian characteristics of the blood could also be taken into account using a constitutive model for viscosity.

One of the contributions of this study to physiology is that it reveals the importance of oscillations in the pressure and flow rate. We see them in figures 6, 9 and 10. It is possible to explain some, but not all, of these oscillations by a simplified network such as ours, which implies that part of the explanation for these oscillations lies in wave propagation in the venous segments and their reflection at major confluences. The reflections we model follow the simple laws arising from the linear theory. There are probably more mechanisms for reflection than we have included in the present model, which could be an interesting point for further study.

Considering the overall structure of predictions and measurements in figures 9 and 10 and disregarding the short-time oscillations, we often find good quantitative agreement with the measurements. This is an indication that the model reproduces correctly the basic mechanism of the muscular pump of the leg: muscle contractions and valvules push blood towards the heart. This is an important result, paving the way for an estimate on the efficiency of various compressive devices. The model is actually used at the time of writing to define new pressure profiles for compression stockings so as to provide specific medical benefits in the case of valvular incontinence. This approach may also be used in medical planning, in particular in the definition of a protocol of clinical trials using the compression devices.

New therapies are appropriate if their risks and benefits compare favourably to those of a reference therapy. Our model can help both to estimate risks and assess benefits. Indeed numerical methods are well suited to the investigation of the venous flows of the lower leg because these flows are difficult to assess using in vivo techniques. Therefore numerical predictions may be useful in evaluating the different blood flows and the clinical measurables (reflux, AVP) that result from the application of different compressive stocking profiles on the lower leg.

Appendix: Wave solutions

This appendix is based on Comolet (1984) and Lighthill (1989). Without loss of generality we may consider the governing equations without gravity or viscous term and with $p_e = 0$

$$\partial_t A + \partial_x (AU) = 0,$$
$$\rho \partial_t U + \rho U \partial_x U = -\partial_x p,$$
$$p = K_p P(A).$$

The equations are linearized by considering small perturbations around the state $U = 0$, $A = A_1$, where A_1 is some reference area. Then

$$\partial_t A + A_1 \partial_x U = 0,$$
$$\partial_t U = -\frac{K_p}{\rho} \frac{\mathrm{d}P}{\mathrm{d}A} \partial_x A.$$

Eliminating U one obtains the wave equation

$$\partial_{tt}^2 A - c^2 \partial_{xx}^2 A = 0,$$

where

$$c^2 = \frac{A_1 K_p}{\rho} \frac{\mathrm{d}P}{\mathrm{d}A}.$$

The same wave equation is obeyed by p and by the flow rate $q = AU$. The general solution can be written as

$$F = f(t - x/c) + g(t - x/c).$$

In particular, if we have

$$p = f(t - x/c) + g(t - x/c),$$

we find that

$$q = \beta \left[f(t - x/c) - g(t - x/c) \right], \tag{A 1}$$

where $\beta = A/c$ is the iterative admittance. We can compute the wave reflections across the confluence. At the connection between the confluence and vessel 1, we have the incident wave $f(t)$ and the reflected wave $g(t)$ so

$$p_1 = f(t) + g(t),$$
$$q_1 = \beta_1 (f(t) - g(t)),$$

and for vessels 2 and 3 we have only the transmitted waves $h_2(t)$ and $h_3(t)$,

$$p_2 = h_2(t),$$
$$q_2 = \beta_2 h_2(t),$$
$$p_3 = h_3(t),$$
$$q_3 = \beta_3 h_3(t).$$

Because the equations are linearized assuming small-enough velocity and area perturbations, any nonlinear term in the confluence equations disappears. Thus, we can simplify the relations at the confluence by considering pressure continuity

$p_1 = p_2 = p_3$ which yields

$$f(t) + g(t) = h_2(t) = h_3(t),$$

and implies that $h_2(t) = h_3(t) = h(t)$. Mass conservation gives

$$\beta_1(f(t) - g(t)) = (\beta_2 + \beta_3)h(t).$$

Using the two previous equations we can compute the ratio between the transmitted and reflecting waves. We have the reflection coefficient R

$$R = \frac{g(t)}{f(t)} = \frac{\beta_1 - (\beta_2 + \beta_3)}{\beta_1 + \beta_2 + \beta_3}, \tag{A 2}$$

and the transmission coefficient T

$$T = \frac{h(t)}{f(t)} = \frac{2\beta_1}{\beta_1 + \beta_2 + \beta_3}. \tag{A 3}$$

From the analytic tube law (2.4 and 2.5) in the positive transmural pressure region

$$p = K_p(A/A_0 - 1), \tag{A 4}$$

and we can compute the area values at the confluence where the pressure is known

$$A_1/A_0 = p/K_p + 1. \tag{A 5}$$

Therefore, the iterative admittance $\beta = A_1/c$ is now (using $c^2 = (A_1/A_0)K_p/\rho$)

$$\beta = \frac{A_1}{c} = A_0 \frac{[\rho(p/K_p + 1)]^{1/2}}{K_p^{1/2}}. \tag{A 6}$$

REFERENCES

Alimi, Y. S., Barthelemy, P. & Juhan, C. 1994 Venous pump of the calf: a stduy of venous and muscular pressures. *J. Vascu. Surg.* **20** (5), 728–735.

Anliker, M., Rockwell, L. & Ogden, E. 1971 Nonlinear analysis of flow pulses and shock waves in arteries. *ZAMP* **22**, 217–246.

Avolio, A. 1980 Multi-branched model of the human arterial system. *Med. Biol. Engng Comp.* **18**, 709–718.

Bassez, S., Chauveau, M. & Flaud, P. 2001 Modeling of the deformation of flexible tubes using a single law. application to veins of the lower limb. *J. Biomech. Engng* **123**, 58–65.

Bernhard, S., Mohlenkamp, S., Erbel, R. & Tilgner, A. 2005 Oscillatory flow in tube with time-dependent wall deformation and its application to myocardial bridges. In *ESAIM: Proceeding* (ed. E. Cancés & J-F. Gerbeau), vol. 14, pp. 25–40.

Bertram, C. D. & Pedley, T. J. 1982 A mathematical model of unsteady collapsible tube behaviour. *J. Biomech.* **15** (1), 39–50.

Brook, Bindi S. 1997 The effect of gravity on the haemodynamics of the giraffe jugular vein. PhD thesis, University of Leeds.

Cancelli, C. & Pedley, T. J. 1985 A separated flow model for collapsible tube oscillations. *J. Fluid Mech.* **157**, 375–404.

Comolet, R. 1984 *Biomecanique Circulatoire*. Masson.

Cros, F. 2003 Confluences, remplissage et vidange: deux aspects singuliers du système veineux jambier. PhD thesis, Université de Paris 7.

Dai, G., Gertler, J. P. & Kamm, R. D. 1999 The effects of external compression on venous blood flow and tissue deformation in the lower leg. *J. Biomech. Engng* **121** (6), 557–564.

Elad, D., Kamm, R. D. & Shapiro, A. H. 1987 Choking phenomena in a lung like model. *ASME J. Biomech. Engng* **109**, 1–9.

Elad, D., Katz, D., Kimmel, E. & Einav, S. 1991 Numerical schemes for unsteady fluid flow through collapsible tubes. *J. Biomed. Engng* **13**, 10–18.

Falson, O. B., Haond, C., Chaslon, M., Moenner, M., Naili, S., Perrault, R., Finet, M. & Ribreau, C. 1998 Endothelial cells in culture: an in vitro model of the wall shear stress gradient effect. *J. Biomech.* **31** (1001), 173–173.

Fernandez, M. A., Milisic, V. & Quarteroni, A. 2005 Analysis of a geometrical multiscale blood flow model based on the coupling of ODEs and hyperbolic PDEs. *Multiscale Model Simul.* **4**, 215–236.

Formaggia, L., Gerbeau, J.-F., Nobile, F. & Quarteroni, A. 2001 On the coupling of 3d and 1d Navier–Stokes equations for flow problems in compliant vessels. *Comput. Methods Applied Mech. Engng* **191**, 561–582.

Formaggia, L., Nobile, F., Quarteroni, A. & Veneziani, A. 1999 Multiscale modeling of the circulatory system: A preliminary analysis. *Comput. Visual. Science* **2**, 75–84.

Fullana, J. M., Cros, F., Flaud, P. & Cros, F. 2003 Filling a collapsible tube. *J. Fluid Mech.* **494**, 285–296.

Fung, Y. C. 1996 *Biomechanics:Circulation*. Springer.

Griffiths, D. J. 1971 Hydrodynamics of male micturation. I. theory of steady flow through elastic walled tubes. *Med. Biol. Engng* **9** (6), 581–588.

Guyton, A. C. & Jones, C. E. 1973 Central venous pressure: physiological significance and clinical implications. *Am. Heart J.* **86** (4), 431–437.

Heil, M. & Pedley, T. J. 1996 Large post-buckling deformations of cylindrical shells conveying viscous flow. *J. Fluids Struct.* **10**, 565–599.

Jan, D. L., Kamm, R. D. & Shapiro, A. H. 1983 Filling of partially collapsed compliant tube. *J. Biomech. Engng* **105**, 12–18.

Kamm, R. D. 1982 Bioengineering studies of periodic external compression as prophylaxis against deep vein thrombosis. Part I: numerical studies. *J. Biomech. Engng* **104** (2), 87–95.

Kamm, R. D. & Pedley, T. J. 1989 Flow in collapsible tube: a brief review. *J. Biomech. Engng* **111**, 177–179.

Kamm, R. D. & Shapiro, A. H. 1979 Unsteady flow in a collapsible tube subjected to external pressure of body forces. *J. Fluid Mech.* **95**, 1–78.

Kimmel, E., Kamm, R. D. & Shapiro, A. H. 1988 Numerical solutions for steady and unsteady flow in a model of the pulmonary airways. *J. Biomech. Engng* **110** (4), 292–299.

Lighthill, J. M. 1989 *Pulse Propagation Theory*, chap. 12, pp. 227–252. SIAM.

MacCormack, R. W. 1969 The effect of viscosity in hypervelocity impact cratering. *AIAA Paper No. 69-454* .

Marzo, A., Luo, X. Y. & Bertram, C. D. 2005 Three-dimensional flow through a thick-walled collapsible tube. *J. Fluids Struct.* **20**, 817–835.

Maton, B., Thiney, G., Dang, S., Tra, S., Bassez, S., Wicart, P. & Ouchene, A. 2006*a* Human muscle fatigue and elastic compressive stockings. *Eur. J. Appl. Physiol.* **97** (4), 432–442.

Maton, B., Thiney, G., Ouchène, A., Flaud, P. & Barthelemy, P. 2006*b* Intramuscular pressure and surface emg in voluntary ankle dorsal flexion: Influence of elastic compressive stockings. *J. Electromyogr. Kinesiol.* **16** (3), 291–302.

Matsuzaki, Y. & Matsumoto, T. 1989 Flow in a two-dimensional collapsible channel with rigid inlet and outlet. *ASME J. Biomech. Engng* **111**, 180–184.

McClurken, M. E., Kececioglu, I., Kamm, R. D. & Shapiro, A. H. 1981 Steady, supercritical flow in collapsible tubes. Part 2. theoretical studies. *J. Fluid. Mech.* **109**, 391–415.

Nicolaides, A. N. & Zukowski, A. J. 1986 The value of dynamic venous pressure measurements. *World J. Surg.* **10** (6), 919–924.

Olufsen, M. S. 1999 Structured tree outflow condition for blood flow in larger systemic arteries. *Am. J. Physiol.* **276** (1 Pt 2), H257–H268.

Olufsen, M. S. 2000 A one-dimensional fluid dynamic model of the systemic arteries. *Stud. Health Technol. Inform.* **71**, 79–97.

Olufsen, M. S., Peskin, C. S., Kim, W. Y., Pedersen, E. M., Nadim, A. & Larsen, J. 2000*a* Simulation and experimental validation of blood flow in arteries with structured-tree outflow conditions. *Ann. Biomed. Engng* **28** (11), 1281–1299.

Olufsen, M. S., Peskin, C. S., Kim, W. Y., Pedersen, E. M., Nadim, A. & Larsen, J. 2000*b* Numerical simulation and experimental validation of blood flow in arteries with structured-tree outflow conditions. *Ann. Biomed. Engng* **28** (11), 1281–1299.

Ozawa, E. T., Bottom, K. E., Xiao, X. & Kamm, R. D. 2001 Numerical simulation of enhanced external counterpulsation. *Ann. Biomed. Engng* **29** (4), 284–97.

Peyret, R. & Taylor, T. D. 1983 *Computational Methods for Fluid Flow*. Springer.

Quarteroni, A. & Formaggia, L. 2003 Mathematical Modelling and Numerical Simulation of the Cardiovascular System. In *Handbook of Numerical Analysis Series, Vol. XII (special volume): Computational Models for the Human Body*, (ed. P. G. Ciarlet & J. L. Lions, guest editor, N. Ayache). Elsevier.

Ribreau, C., Naili, S. & Langlet, A. 1994 Head losses in smooth pipes obtained from collapsed tubes. *J. Fluids Struct*. **8**, 183–200.

Rosar, M. E. & Peskin, C. S. 2001 Fluid flow in collapsible elastic tubes: a three-dimensional numerical model. *N.Y. J. Math*. **7**, 281–302.

Shapiro, A. H. 1977 Steady flow in collapsible tubes. *ASME J. Biomech. Engng* **99**, 126–147.

Sherwin, S. J., Franke, V., Peiro, J. & Parker, K. 2003 One-dimensional modelling of vascular network in space-time variables. *J. Engng Math*. **47**, 217–250.

Stergiopulos, N., Young, D. F. & Rogge, T. R. 1992 Computer simulation of arterial flow with applications to arterial and aortic stenoses. *J. Biomech*. **25**, 1477–1488.

Stettler, J. C., Niederer, P. & Anliker, M. 1981 Theoretical analysis of arterial hemodynamics including the influence of bifurcations. Part I: mathematical models and prediction of normal pulse patterns. *Ann. Biomed. Engng* **9** (2), 145–164.

Wan, Jing, Steele, Brooke, A., Sean, Strohband, Sven, G. R. Feijóo, Hughes, Thomas J. R. & Taylor, Charles A. 2002 A one-dimensional finite element method for simulation-based medical planning for cardiovascular disease. *Comput. Methods Biomech. Biomed. Engng* **5** (3), 195–206.

Wang, J. J. & Parker, K. H. 2004 Wave propagation in a model of the arterial circulation. *J. Biomech*. **37** (4), 457–470.

Westerhof, N., Bosman, F., Vries, C. & Noordergraaf, A. 1969 Analog studies of the human systemic arterial tree. *J. Biomech*. **2**, 121–143.

Wild, R., Pedley, T. J. & Riley, D. S. 1977 Viscous flow in collapsible tubes of slowly-varying elliptical cross-section. *J. Fluid Mech*. **81**, 273–294.

Young, D. F. & Tsai, F. Y. 1975 Flow characteristics in models of arterial stenosis. I. steady flow. *J. Biomech*. **6**, 395–410.